JOURNAL OF OPTOELECTRONICS AND ADVANCED MATERIALS Vol. 19, No. 11 - 12, November – December 2017, p. 679 - 687

Analytical approaches to predict the different guiding regimes for the design of SCPCFS and their applications

G. LATHA*, PRITA NAIR
Department of Physics, SSN College of Engineering, Chennai, India

Modeling of optical guidance properties of commercial solid core photonic crystal fiber (SCPCF) and an estimation of some of their salient performance metrics has been carried out using a combination of simple TMM technique and geometry based equivalent single mode modeling. These have been validated and supplemented by FEM analysis and experimental analysis of mode patterns.

(Received April 3, 2017; accepted November 28, 2017)

Keywords: SCPCF, Infiltration, PCF Modeling

1. Introduction

Plane wave expansion method (PWE), beam propagation method (BPM), finite difference time domain method (FDTD), effective index approach and full-vector finite element method (FEM) are some of the techniques used for numerical modeling of photonic crystal fibers (PCFs) [1]. FDTD and FEM are universal methods for modeling all types of fibers, whereas BPM is probably the best choice for modeling longitudinally varying PCFs. The most widely used method, FEM, enables estimation of the fundamental parameters (effective index of the modes, mode field diameter (MFD)) and the confinement properties of PCF. Theoretical modeling of the PCF in this work uses a combination of two simple computationally efficient analytical modeling techniques to predict these fundamental metrics and the different guidance regimes of solid core PCFs. These methods can be used for the design and prediction of different applications, reducing the dependence on computationally intensive FEM /FDTD modeling. The main analytical modeling techniques used are the

(i) transfer matrix method (TMM), where the transmission characteristics of the SCPCF is modeled in terms of the transfer functions of the two key 1D photonic band gap (PBG) structures representing the PCF microstructure and

(ii) geometry based effective cladding index modeling technique which takes into account the degree of porosity of the cladding microstructure and the refractive index of the fluid filling the pores.

The TMM method is used to predict the different transmission regimes in the PCF, namely the index guided region, PBG region and the lossy cladding guided/multi-waveguide region. It can predict the low loss transmission windows through the PCF as a function of the source wavelength (for a given fluid infiltrate), or the index of the fluid filling the PCF (for a given source wavelength). Geometry based method, on the other hand, can be used to predict the effective indices and MFDs of the Gaussian core mode in the index-guided regime of the PCF.The knowledge of the effective indices can also lead to an estimation of the dispersion characteristics of the PCF. The results of these methods have been compared to those obtained through finite element analysis of the propagation of the electromagnetic waves through the PCF, using COMSOL Multiphysics. Two major parameters that cannot be visualized/ estimated by these analytical methods are the mode field patterns and the losses, though its prediction can still be made.

2. TMM approach for modeling PCFs

This section describes the TMM technique used to model the propagation of the electromagnetic field through a SCPCF comprising of air or fluid filled holes in a host matrix of silica. Fig. 1 depicts the schematic of the cross-section of the LMA-20 SCPCF (Thor Labs) with its air-filled micro holes. This SCPCF has six layers of hexagonally arranged holes of diameter h of 6.4 μm and pitch Λ of 13.2 μm. The omnidirectional structure of the LMA-20 can be analysed in terms of two photonic bandgap (PBG) structures. It can be seen that along all the axes passing through the opposite vertices (e.g.Γ-X, Γ-K directions in Fig.1), of the central innermost hexagonal layer of air-holes represented by orange dashed lines, the periodic pattern consists of six bilayers of silica/air on either side of the central defect region (core).The other set of distinct periodic structures are the ones along the centre of the hexagonal sides of the core region (Γ-M direction).

Thus the cladding microstructure with central core region can be modeled in terms of these two sets of 1D PBGs along the X and Y directions. The 1D photonic bandgap structure (PBG) in these directions is also shown in Figure 1.Here d_x, d_y are the thickness of the silica layer in the X and Y directions, h the diameter of the micro holes and d_{xd}, d_{yd} the dimension of the central silica core in

the X and Y directions. The PBGs have 25 layers along X-axis and 13 layers along Y-axis.

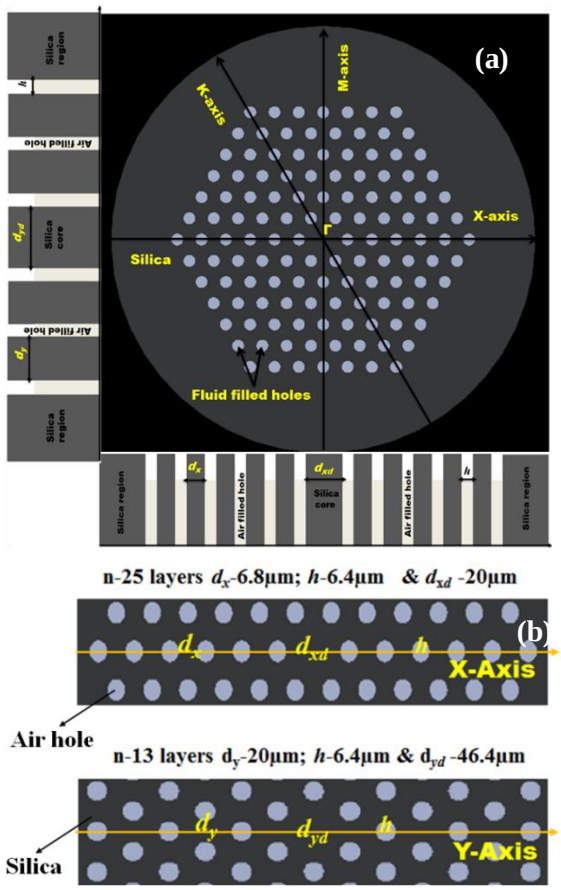

Fig. 1. (a) Cross-section of LMA -20 PCF and 1(b) one dimensional PBG of LMAPCF

Alternatively, these PBGs in the X and Y directions can also be modeled as Fabry-Perot resonators, with the core as the central resonator flanked on either side by two identical PBG mirrors comprising of 12 layers and 6 layers respectively. The stop bands in the transfer function of these PBGs are the modes that are not coupled out through the micro-structured cladding (anti-resonant modes) and are hence the frequencies that are confined in the core of the PCF. The effect of higher index fluids infiltrated into the microholes on the optical guidance through the PCF core can be easily taken into account in the model by appropriately varying the refractive index of the fluid filling the hole. In the TMM method [4], the response for forward and backward travelling electromagnetic waves at the interface between a pair of dielectric media is taken into account using the interface matrix M_I, whose elements are written in terms of the Fresnel reflection and transmission coefficients for that interface. The travel through each medium is represented by the propagation matrix, M_p, which incorporates the phase change of the waves due to travel. If E_i and E_j' represent the electric fields in layers 'i' on left and 'j 'the right of the interface n, + and – suffixes of these fields indicate the forward (left to right), and backward travel (right to left) directions respectively, r_{ij}=-r_{ji} & t=t_{ij}=t_{ji} the reflection and transmission coefficients across interface n, μ_j & d_j the refractive index and thickness of the layer j, and M_I^n the interface matrix of the n^{th} interface, then the interface response at n^{th} layer and M_p^j the propagation matrix of j^{th} layer are represented by the equations

$$\begin{bmatrix} E_{i+} \\ E_{i-} \end{bmatrix} = M_I^n \begin{bmatrix} E_{j+}' \\ E_{j-}' \end{bmatrix} \text{ where } M_I^n = \frac{1}{t}\begin{bmatrix} 1 & r_{ij} \\ r_{ij} & 1 \end{bmatrix}$$
$$M_P^j = \begin{bmatrix} e^{i\delta} & 0 \\ 0 & e^{-i\delta} \end{bmatrix} \text{ where } \delta = \frac{2\pi}{\lambda}\mu_j d_j \quad (1)$$

The propagation through a multilayer structure is represented by sequentially multiplying the appropriate matrices.

2.1. Results and analysis of TMM modeling

The transmission characteristics of representative 1D PBGs of LMA-20 has been numerically simulated using MATLAB with dispersion of silica accounted for using Sellemeir's equation with appropriate coefficients [6]. Fig.2 shows the transfer function of electromagnetic waves through the air-filled cross-section of LMA-20 PCF. The wavelengths for which the transmission is nearly zero are those which are guided with minimal loss in the PCF. The two PBG structures along the X and Y axis of the PCF have their transmission minima at slightly different wavelengths because of the change in their periodicity.

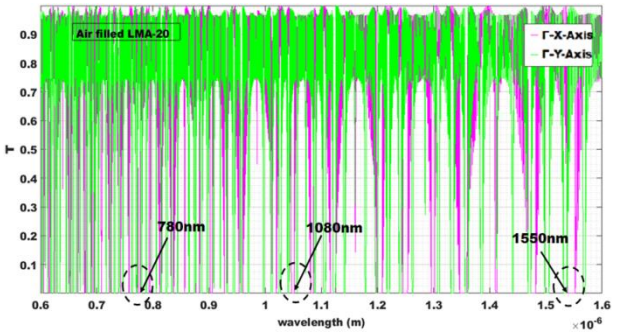

Fig. 2. Transmission spectra of air-filled LMA-20

.

The transfer function shows that LMA-20 guides most of the wavelengths between 650nm and 1600nm, indicating the endlessly single mode nature of the PCF. However, the periodicity of the transmission minima's increase with increase in wavelength. This is typical of Fabry-Perot resonators wherein the transmission peaks occur whenever the defect layer thickness is equal to integral multiples of $\lambda\mu_d(\lambda)/2$ where $\mu_d(\lambda)$ represents refractive index of the defect layer i.e. silica at the specific wavelength. Low loss core guidance (where transmission is zero) occurs in bands near 780 nm, 1080 nm and 1550 nm. This result is in agreement with the LMA-20 data sheet which shows these to be its optimized wavelengths with minimum attenuation. As an illustration, Fig. 3 gives an enlarged view of the transmission spectrum close to 1550 nm showing that in the 1.51 -1.53 µm range the

losses due to transmission through the microstructured cladding is more and core guidance is comparatively much better in the 1.532 μm to 1.552 μm bands.

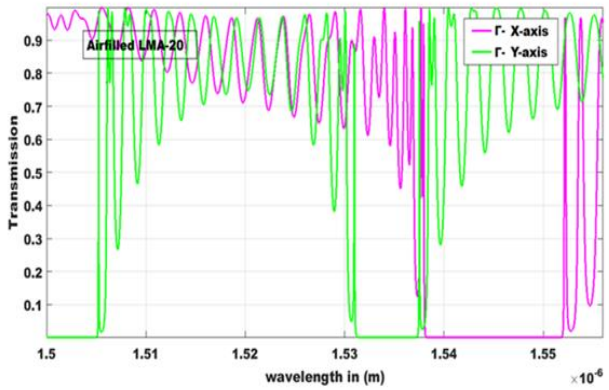

Fig. 3. Expanded view of the transfer function of LMA-20 in the 1.5-1.55μm region

Applications of SCPCFs in dispersion control, sensors etc. exploit the direct accessibility to the light guided by the SCPCF provided by the micro-holes. This control is affected by infiltration of the micro-holes with fluids/solids of different refractive index. When the micro-holes in the cladding are filled with fluids of slightly higher index, the power confinement in the core will decrease and as the fluid RI approaches the silica refractive index, the loss will increase drastically. At much higher fluid RI values, core silica region will be surrounded by a microstructured cladding with larger effective index. For sufficiently high index contrast, this should lead to bandgap based guidance. Numerical simulation of the PBGs, changing the refractive index (RI) of the fluid infiltrated into the holes from 1.0 to 1.9 has been carried out to predict these guidance regimes.

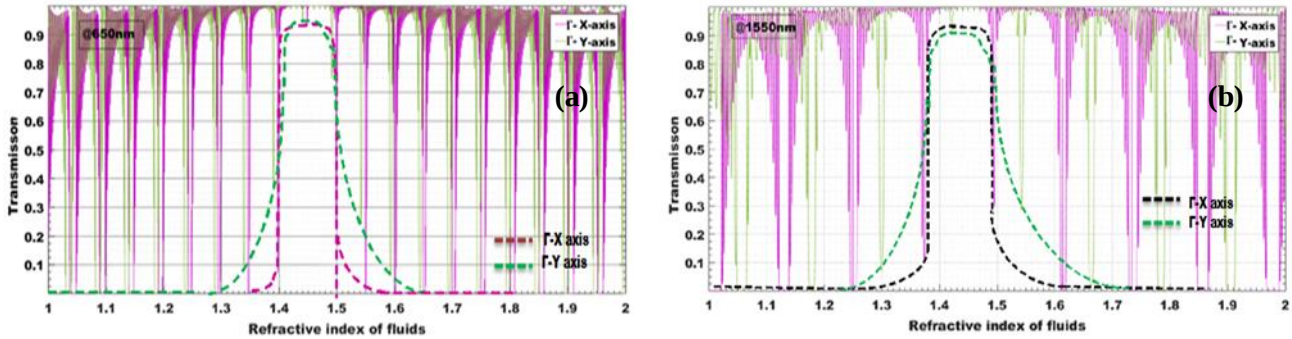

Fig. 4. Variation of transmission through fluid-filled SCPCF MA-20 with increasing fluid RI for (a) 650 nm (b) 1550 nm

The transfer function at 650 nm and 1550 nm for varying fluid RI is plotted in Fig. 4(a) & 4(b).For source wavelength of 1550 nm, the fluid indices (n_{fluid}) at which low loss transmission windows occur, have a periodicity of 0.13 RIU starting from that of air (RI=1) whereas it occurs at a smaller interval of 0.05 RIU at 650 nm.

For each source wavelength, the bandwidths of these low loss windows increase with increase in index contrast, $|n_{silica} - n_{fluid}|$, and source wavelengths. The envelope of the transmission curves shown with dashed lines in Fig.4 indicate lower transmission through the cladding (or larger confinement of core modes) for fluid RIs in the 1.0-1.35 and 1.6-2.0 ranges. The former can be attributed to the index guided regime and the latter due to PBG based guidance. For RI values closer to the silica wavelength i.e. 1.4-1.5, the transmission through the cladding region is nearly 90% indicating that power will no longer be guided through the PCF core. The difference in the transmission windows with source wavelengths is due to the dispersion of silica. Lower RI at the higher source wavelengths lead to lower index contrasts and larger MFDs apart from the shift of the lossy cladding guided region to lower fluid RIs. As PBG based guidance can give negative dispersion, this study with higher index fluid infiltrate in the micro-holes can be used to predict the n_{fluid} at which negative dispersion can be expected. For example a comparison of Fig. 4 (a) and (b) shows that an n_{fluid} of 1.75 or 1.9 will give negative dispersion at 1550 nm. The allowed variation of fluid RI around these values will be more for the higher n_{fluid} value. As per the TMM results in this region, confinement along the axis connecting the opposite vertices of the innermost hexagonal pattern is weaker than perpendicular to the hexagonal faces. So mode patterns can be expected to show more leakage of power into the cladding along the vertices of the first hexagonal layer of holes defining the core boundary.

Thus the TMM based analysis is able to

(i) identify clearly the low loss transmission bands of the PCF. Identify the index guided and PBG guided low loss regimes in the case of fluid infiltrated LMA-20 for any source wavelength

(ii) obtain qualitative idea of mode patterns from the knowledge of where power confinement can be expected

(iii) identify possible regions where negative dispersion characteristics can be expected based on the location of the PBG regimes.

Quantitative estimate of the complex effective index of the propagating Gaussian core mode, mode patterns and MFDs will however require alternate methods like FEM or equivalent analytical expressions. Confirmation of mode patterns and losses through FEM studies has been used to further validate the predictions of TMM studies.

2.2. Validation through FEM modeling of LMA-20 PCF

COMSOL Multiphysics, version 4.4a with the RF module, was employed to model LMA-20. Mode field patterns, effective indices and MFDs of the core modes with air-filled and high-index filled holes have been studied. Effective indices with real part close to that of silica at 650nm and no imaginary part indicates very low transmission loss values. This is observed for air-filled and low-index filled holes where mode patterns show strong confinement in the core. The same trend in the effective index and mode pattern is also observed at a high fluid index of 1.9 where TMM predicts PBG based core guidance.

The Fig .5 shows that when infiltrated fluids RI (n_{fluid}) is 1.456 i.e. close to that of silica, the imaginary part is $1.176x10^{-6}$ indicating losses due to transverse power transmission into the silica cladding region. When n_{fluid} is 1.6734, the FEM results show that the field is restricted to a few high index fluid-filled micro-holes to the periphery of the microstructure and the secondary silica cladding region, resulting in losses which are 2.49 times more. A comparison with the TMM simulation results at 650 nm shows that at n_{fluid} values where the FEM predicts a complex effective index, TMM also predicts high transmission losses. For n_{fluid} values at which transmission losses are less than 10%, mode patterns obtained from FEM confirms the strong confinement in the silica core of the PCF.

Fig. 6 shows the mode patterns as an inset in the appropriate region of the transfer function predicted by TMM. The mode patterns illustrate optical power confinement in the (i) core in the index guided regime (Region I) (ii) silica region including those in the cladding (region II) (iii) high index micro-holes (Region III) and (iv) core again due to PBG guidance. Complex effective index of mode and transmission losses for some representative values for RI of fluids infiltrated into LMA-20are depicted in Table 1.

Table 1. Complex effective index of mode and transmission losses for some representative values for RI of fluids infiltrated into LMA-20

RI of infiltrate (n_{fluid})	Effective index of mode from FEM analysis	Transmission loss (%)from TMM studies
1.347	1.4564	8.41
1.456	1.45642 - i1.175835e-06	100
1.6734	1.456328- i2.928431e-06	96.13
1.9	1.456396	9.13

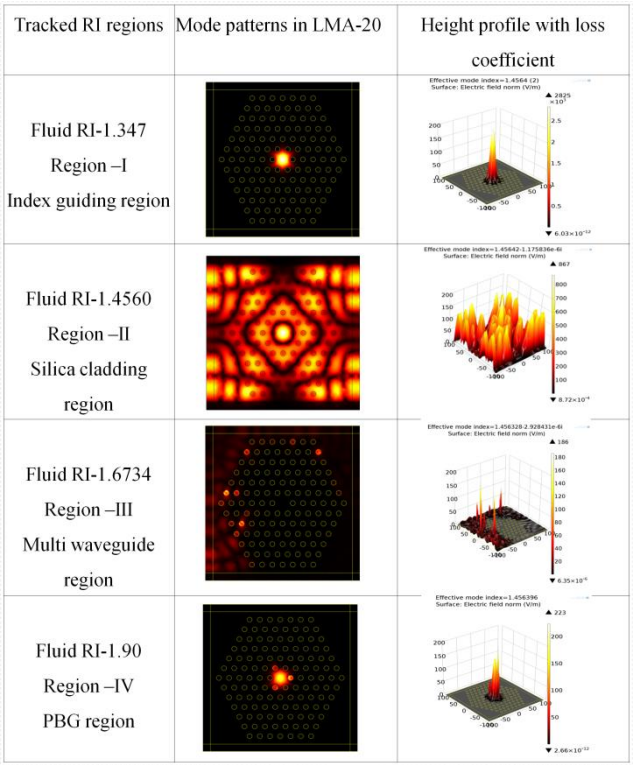

Fig. 5. Simulated mode patterns for different guidance regimes of LMA-20

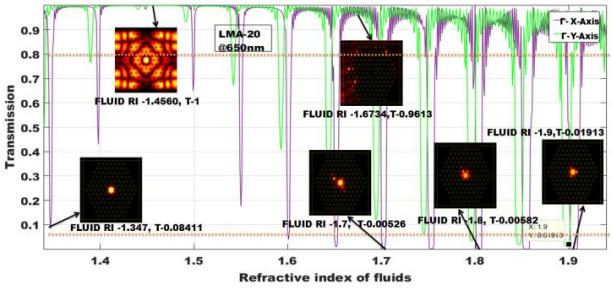

Fig. 6. Transmission spectra with FEM based mode patterns in different guiding regimes

FEM modeling allows one to extract all critical parameters of the transmission characteristics of the PCF. As these are computationally intensive, especially when parametric sweeps and optimization runs need to be done, it will be more efficient to do the FEM modeling only for specifically identified critical regions. The agreement of the FEM results to the predictions from TMM shows that TMM modeling can serve as an initial guideline for selecting regions of specific interest for developing applications.

3. Geometrical modeling of LMA-20 PCF

Analytical modeling of PCF as an equivalent single mode fiber can be done using the knowledge of the geometry of the PCF. In a solid core PCF, porosity '*p*', of the hexagonal micro-structured cladding can be defined as the ratio of the sum of the area of micro holes to the total area of the microstructured cladding of a fiber. In terms of n_{fluid} and n_{silica}, the refractive indices of the fluid in the micro hole and the silica respectively, the effective index of the microstructured cladding ($n_{effclad}$) can be defined as

$$n_{eff\,clad} = (p * n_{fluid} + (1-p) * n_{silica}) \quad (2)$$

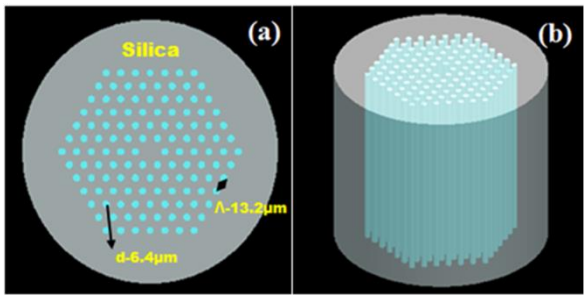

Fig. 7. Cross section of LMA-20 (a) 2D view& (b) 3D view

Modeling the refractive index of the micro cladding in terms of the index of the silica region and the index of the fluid filling the pores enables an easy extension of this model to an application of sensors with analyte infiltrated into the pores. The 2D cross-section and 3D view for SCPCF fiber with the geometrical parameters as specified by the manufacturer for the LMA-20 with core diameter 20 μm are illustrated in Fig. 7.The porosity of LMA-20 SCPCF calculated from its geometry is 0.2554 and hence its effective cladding index as a function of RI of fluid can be represented by Equation 3 given below.

$$n_{eff\,clad}(\lambda) = (0.2554 * n_{fluid} + 0.7446 * n_{silica}(\lambda)) \quad (3)$$

3.1. Estimation of V- number, effective index of lower order Gaussian mode and MFD

The V number of the PCF with pitch Λ can be estimated using the equation (Nielsen et al 2003)

$$V_{PCF}(\lambda) = \frac{2\pi}{\lambda}\Lambda\sqrt{\left(n^2_{silica}(\lambda) - n^2_{effclad}(\lambda)\right)} \quad (4)$$

In analogy with single mode fiber [1],solving transcendental Equation 5 for the value of '*b*' parameter which satisfies the relationship for the lowest order mode, the effective index of the guided mode n_{eff} at the wavelength of interest can be calculated using Equation 6. In this calculation, V-number (normalized frequency) of the single mode fiber is replaced by the $V_{PCF}(\lambda)$. *J* and *K* represent the Bessel functions of the first and second kind respectively.

$$V\sqrt{(1-b)}\frac{J_1\left[V\sqrt{(1-b)}\right]}{J_0\left[V\sqrt{(1-b)}\right]} = V\sqrt{b}\frac{K_1\left[V\sqrt{b}\right]}{K_0\left[V\sqrt{b}\right]} \quad (5)$$

$$n_{eff}(\lambda) = \sqrt{n^2_{effclad}(\lambda) + b\left(n^2_{silica}(\lambda) - n^2_{effclad}(\lambda)\right)} \quad (6)$$

The value of '*b*' for which LHS is equal to RHS in Equation 5 is evaluated by finding the value of '*b*' for which S=LHS-RHS=0, through numerical simulation. Illustrative samples of the value of '*b*' represented graphically for n_{fluid}=1 is shown in Fig.8 along with the *V* values for 650nm wavelength.

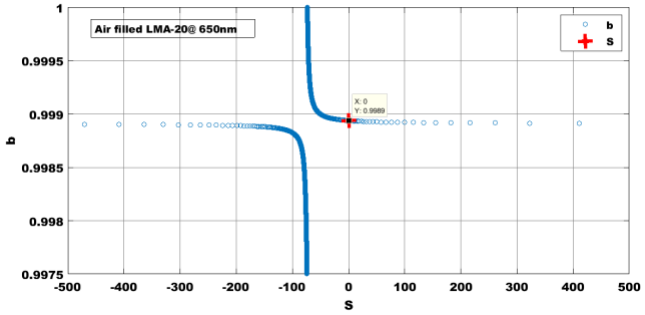

Fig. 8. Estimating b-parameter for LMA-20 @650nm for n_{fluid}=1.0

This model can also be used to predict the n_{eff} values with the micro holes filled with fluids of higher index. A comparison of the effective index of the guided lower order modes calculated using equation 6 for LMA-20 from its geometrically determined V_{PCF} and that estimated using FEM is given in Table 2.The error with respect to FEM values are within $\pm 1.6\text{x}10^{-5}$ or the error% is $1.1\text{x}10^{-3}$. Fig.9 illustrates graphically the extraction of *b* value with n_{fluid} of 1.3 at 650 nm.

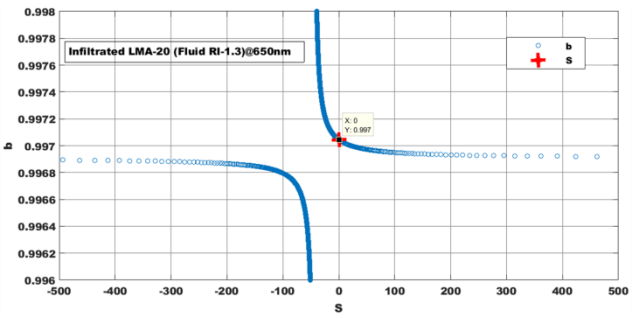

Fig. 9. Estimating b-parameter for LMA-20 @650nm for n_{fluid}=1.

Table 2. V-parameter and effective index estimates for the LMA-20PCF

Wavelength in nm	LMA-20		
	V_{PCF}	n_{eff} (FEM)	n_{eff} (Analytical Fit)
650	72.73	1.456397	1.456400
750	62.83	1.454057	1.454040
850	55.3	1.452268	1.452249
950	49.38	1.450778	1.450758
1050	44.6	1.449450	1.449428
1150	40.65	1.448203	1.448180
1250	37.41	1.446989	1.446964
1350	34.58	1.445775	1.445748
1450	32.14	1.444540	1.444511
1550	30.01	1.443269	1.443237

The concurrence between the n_{eff} estimates using equation 6 and FEM analysis suggests that this geometry dependent calculation of $n_{effclad}$ and hence V_{PCF} can be used instead of rigorous FEM modeling. The calculated V_{PCF} can also be used to estimate MFD of the lowest order mode, provided coefficients in the expression for mode field radius equation can be fit empirically. Mode field radius can be fit from V_{PCF} values using the standard expression [2], where coefficients A, B, C depend on the index profile of the PCF and 'g' determines the shape of the index profile.

$$\omega = \Lambda\left(\frac{A}{V_{PCF}^{2/(2+g)}} + \frac{B}{V_{PCF}^{3/2}} + \frac{C}{V_{PCF}^{6}}\right) \quad (7)$$

The profile number 'g' influences the index profile across the cross-section of the PCF. The expression for the RI profile adopted from standard single mode fiber in terms of variation of RI with distance (x), measured from the centre of the core, is given by

$$n(x) = n_{silica}[1 - 2\Delta)\left(\frac{x}{\Lambda}\right)^{g}]^{2} \quad (8)$$

Where a= radius of the core=Λ, $\Delta = \frac{(n_{silica} - n_{effclad})}{n_{silica}}$ and g- profile index number.

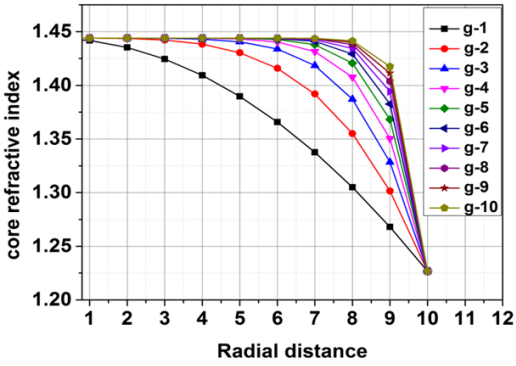

Fig. 10. Variation in RI profile with g parameter

Fig. 10 shows that values of g=8 or above, RI profiles are nearly rectangular. Therefore a g value of 8 is chosen for the fitting. In order to ensure that the coefficients are appropriate for all source wavelengths, the best fit was arrived at by solving a set of simultaneous equations for MFD at different wavelengths for the LMA-20 SCPCF. For this calculations, the MFD as a function of wavelength has been extracted from the datasheets provided by the manufacturer. The coefficients providing the best fit to these MFD values are shown in Table3.The MFDs calculated with the A, B, C coefficients are given in Table3, are able to reproduce the MFD values in the data sheet within an error percentage 0.834% for commercial LMA-20.The variation in V_{PCF} values and MFDs with wavelength and its agreement with the manufacturer's data and those computed using FEM analysis is tabulated in Table 4 for LMA -20

Table 3. A, B, C coefficients for LMA-20

LMA Family	'A'	'B'	'C'
LMA-20	1.5663	-32.075	2.5490 e^{7}

Infiltration of the porous area with fluids in the 1.0-2.0 RI range, leads to a change in the effective cladding index over a range of 0.255RIU. The value of infiltrated fluids RI at which the cladding effective index becomes equal to that of the silica core indicates the end of the index guided regime of the SCPCF as at this value, optical power spreads into the cladding region. The reduction in the index contrast of the core with effective cladding index also increases the MFD of the lowest order mode of PCF.

Assuming that the values of A, B, C coefficients holds good even when n_{fluid} changes, the V-parameter and MFDs for different fluid RIs has also be estimated, for n_{fluid}<n_{silica}. Table 5 gives the V-parameter and MFDs calculated for different n_{fluid} values for LMA-20 for input optical power at 650 nm. As n_{fluid} increases, the MFD increases indicating lower confinement and hence spread of power over larger areas. As per the calculations in this approach, for values of n_{fluid} >1.41 the MFD exceeds the core diameter of 20 µm, indicating non-zero power in the silica cladding. This limit on the fluid RI estimated from this approach agrees well with the predictions of TMM modeling and is also confirmed by the mode patterns simulated using COMSOL. The error in the analytical fit for MFDs is found to be smaller if the PCFs have larger slopes in the variation of MFD with wavelength. The error% in MFD estimation using the same procedure is found to be smaller (~0.57) for LMA-10 and LMA-8.

Table 4. Wavelength versus MFD in LMA-20 PCF with error %

Wavelength in nm	V_{PCF}	MFD in µm			Error % (Analytical FIT)	Error % (FEM)
		(Data sheet)	(Analytical FIT)	(FEM)		
650	72.73	16.320	16.184	16.181	0.8334	0.85
750	62.83	16.360	16.377	16.211	0.1039	0.91
850	55.3	16.399	16.498	16.240	0.6036	0.96
950	49.38	16.466	16.564	16.268	0.5902	1.20
1050	44.6	16.492	16.59	16.296	0.5917	1.18
1150	40.65	16.532	16.592	16.326	0.3629	1.24
1250	37.41	16.585	16.585	16.354	0	1.39
1350	34.58	16.624	16.587	16.381	0.2261	1.46
1450	32.14	16.636	16.621	16.410	0.0913	1.35
1550	30.01	16.717	16.659	16.438	0.3481	1.64

Table 5. V-parameter and MFD for LMA-20 for different fluid RIs at 650 nm

RI of fluids	V-Parameter	MFD (Analytical Fit) in µm
1	72.82	16.18
1.1	64.64	16.59
1.2	55.08	16.75
1.3	43.21	16.84
1.4	26.08	17.58
1.41	23.67	18.71
1.42	20.98	21.9
1.43	17.88	33.13
1.44	14.11	95.09

In order to experimentally validate the guidance regimes predicted by TMM modeling, the mode patterns at the output of four dedicated LMA-20 fiber samples, with the cladding micro-structure infiltrated with RI of (i) 1.36±0.005 (ii) 1.46±0.005 (iii) 1.47±0.005 have been recorded and reported[13] using 650 nm as the laser source. As predicted by the TMM, the first two mode patterns indicate guidance in the PCF core, providing proof of index guided region and the third sample shows a mode pattern where the power is confined in the holes in the cladding again validating the predictions of TMM.

Table 6 Comparison of variation in MFD values by experiment, FEM &Geometry based modeling@650 nm

LMA-20SCPCF	MFD in microns		
	Experiment	FEM	Analytical
With Air holes (RI =1.0)	16.2 ± 0.74	16.181	16.433
With fluid (RI =1.36±0.005)	16.406 ± 0.74	16.374	16.608

In the first two cases, MFD values have also been extracted from the experimentally recorded mode patterns using image processing technique given in detail in [13]. This technique has been further modified to improve the background white light subtraction, and the results obtained are given in Table 6. The MFD values obtained from experiment, FEM simulations and analytical modeling are given in Table 6. The analytical model predicts the MFD for air-filled LMA-20 with a maximum error percentage of 0.834% and the FEM modeling predicts the MFDs with a maximum error percentage of 1.64% with reference to those provided in the data sheet. The data sheet of LMA-20 gives the MFD at 650 nm for air-filled holes to be around 16.32±1.5 µm and the experimental results are within this error margin.

As chromatic dispersion calculation is based on effective indices, it has also been used for validation of the analytical modeling done in this paper. Chromatic dispersion values (CD) for air-filled LMA-20SCPCF have been estimated from the effective indices calculated using

the geometry based analytical technique and verified by comparing with those mentioned in data sheets by the manufacturer (refer to Table 7) and COMSOL based FEM analysis.

Table 7. Comparison of variation in CD values by FEM, from Data sheet & by Geometry based modeling

LMA-20 (Wavelength in nm)	Dispersion in ps/nm/km		
	FEM results	From Data sheet	Analytical results
1550	51.67	49.55	51.60
1570	52.34	50.78	52.30
1590	52.83	51.88	53.0

4. Conclusions

Numerical modeling of LMA-20 SCPCF has been done using a combination of TMM and analytical modeling as an equivalent single mode fiber, with an effective cladding index calculated based on porosity & index of materials filling the holes of the microstructured cladding. Most of the metrics of the PCF, the real part of the effective index of the modes, MFDs and identification of the main guidance regimes, the index guiding and PBG guiding regimes and a qualitative idea about the losses of the modes have all been estimated using these studies. These have been further verified and supported through COMSOL Multiphysics based FEM modeling. The simple geometry based analytical technique predicts effective index values of the lowest order index-guided mode with a maximum error % of 10^{-3}, and MFDs with its variation with RI of infiltrate with a maximum error % of 0.834 when compared to FEM. The estimated effective index values have also been used to verify the chromatic dispersion reported in the data sheet of LMA 20. Mode patterns of air-filled and fluid infiltrated LMA 20 and MFDs extracted from them [13] provide experimental support to the modeling and the application of this technique to model RI sensors using PCFs.

The variations in the transmission characteristics of the solid core PCFs due to temperature and strain can be easily incorporated into the TMM and geometry based analytical technique as a change in the RI of silica and fluid through their thermo-optic and stress-optic coefficients respectively. However, the sensitivity of air filled solid core PCFs are very low because of the low thermo-optic and stress optic coefficients of pure silica (of the order of 10^{-6} and 10^{-11}[15] respectively.

The techniques used in this paper can model optical guidance through solid core PCFs with the holes in the microstructure fully or selectively infiltrated [24] with fluids of high or low RI. Therefore applications of solid core PCFs like sensing, dispersion control (Dehghan F et al 2010, Redwan Ahmad et al 2013) and resonance induced mode transformations can be modeled using the techniques reported here. Temperature sensors using high temperature coefficient fluid infiltrates, capable of giving effective index changes of ~ 10^{-6} RIU and therefore sensitivities of $-166\,pm/°C$ as reported by [Sun-jie Qiu et al. 2012, Latha G, and Prita Nair 2014] can be easily modeled using these techniques. Tapered sections of large mode PCFs of appropriate geometry, or special geometrical designs, can be evaluated quickly through TMM modeling to identify wavelength bands where dispersion will be negative. Alternatively it can also be used to identify the fluid infiltrate that can provide nearly omnidirectional low loss PBG guidance at the wavelength of interest, which can be used for realization of dispersion compensators as the fibers exhibit a high negative dispersion (Maji et al. 2013) in this wavelength. If fluid infiltration is restricted to the holes that form the core boundary they can provide mode shape transformations. Large mode area PCFs tapered to appropriate dimensions and infiltrated with material of appropriate RI or even metal (as they give reflectance due to surface plasmon resonances), can serve as 3D mode transformers that can couple optical power from large circular spot size sources to small rectangular planar integrated optics platforms.

References

[1] Ajoy Ghatak, K.Thayagarajan, Introduction to Fiber Optics, 2007.
[2] M. D. Nielsen, N. A. Mortensen, J. R. Folkenberg, A. Bjarklev, Optics Letters **28**, 2309 (2003).
[3] K. Saitoh, M. Koshiba, Journal of Lightwave Technology **23**(11), 3580 (2005).
[4] S. J. Orfanidis -Electromagnetic Waves and Antennas.pdf.
[5] G. A. Agrawal, Nonlinear Fiber Optics, 2nd edition, Elsevier, 1995.
[6] G. Ghosh, Appl. Opt. **36**(7), 1540 (1997).
[7] R. Hadley, R. E. Smith, J. Quantum Electron. **13**, 465 (1995).
[8] J. C. Chen, S. Jungling, Opt. Quantum Electron. **26**, S199 (1994).
[9] K. S. Yee, IEEE Trans. Antennas Propagation **AP-14**, 302 (1966).
[10] A. Taflov, "Computational Electrodynamics: The Finite Difference Time Domain Method." Norwood, MA: Artech House 1995, p. 1006.
[11] A. Gautam Prabhakar, B. Akshit Peer, C. Ajeet Kumar, D. Vipul Rastogi, Finite Element Analysis of Solid-Core PhotonicCrystal Fiber, Students Conference on Engineering and Systems**,** 12728808, Allahabad, UP, India**,** March (2012).
[12] K. Saitoh,M. Koshiba, IEEE Journal of Lightwave Technology **23**, 3580 (2005).
[13] G. Latha, Prita Nair, OPTIK –International Journal for Light and Electron Optics **127**, 10991 (2016).
[14] G. Latha, Prita Nair, Proceedings of the COMSOL International Conference, Bangalore, India, 4-5 November (2014).

[15] A. J Barlow, D. Payne, IEEE J of Quantum Electron, QE-19 **5**, 834 (1983).
[16] Redwan Ahmad, A. H. Siddique , Md. Sharafat Ali, Aminul Islam, K. M. Nasim, M. Samiul Habib, International Conference on Electrical Information and Communication Technology (EICT) (2013).
[17] Sun-jie Qiu, Ye Chen, Fei Xu, Yan-qing Lu, Optics Letters **37**, 863 (2012).
[18] P. J. Bennett, T. M. Monro, D. J. Richardson, Opt. Lett. **24,** 1203 (1999).
[19] Limin Xiao, Wei Jin, Senior, Yiping Wang, Chun-Liu ZhaoJournal of Lightwave technology **25,** 3563 (2007).
[20] Chen. Z. C. Xiong, L. M. Xiao, W. J. Wadsworth, T. A. Birks, OSA/CLEO/IQEC (2009).
[21] T**.** Birks, A. Witkowska, S. Leon-Saval, K. Lai, W .Wadsworth, 9th International Conference on Transparent Optical Networks, ICTON (2007).
[22] Z. Chen, Xi Xiaoming, Z. W. Jing, Z. F. Jiang, Journal of Lightwave Technology **29**, 3744 (2011).
[23] F. Dehghan, M. Ebnali-Heidari, Q. Shi, IEEE Winter Topicals, Keystone, Colorado, USA (2011).
[23] Boris T. Kuhlmey, Benjamin J. Eggleton, Darran K. C. Wu, Journal of Lightwave Technology **27**, 1617 (2009).
[24] P. S. Maji, P. R. Choudhary, ISRN Optics **13**, 1 (2013).

Addendum: Information on PCF handling

The application note on how to strip, cleave and splice and PCFs brought out by NKT Photonics the main manufacturer of PCFs serve as a guideline to handle PCFs. Unlike the standard SMF, the microstructure of the cladding in a solid core PCF generally prevent the free propagation of crack induced cleavage plane making cleaving of PCFs a slightly more difficult task. Vytran cleavers and splicers recommended by the manufacturers are the best choice though they are costly. However, with enough practice this can also be achieved manually as can be seen from our images of fiber cross-section [13]. Secondary suppliers like Thor labs have come up with ceramic ferrules, FC/PC mating sleeves and quick release interconnects that can be used to connect PCFs of different sizes. These ferrules have outer diameters compatible with standard FC/PC connectors and can hence be used to connect to sources, OSA, power meter or to butt couple to SMF fibers. Butt coupling efficiencies to SMFs are only 10% and therefore a telescope like double lens arrangement will be more suitable for SMF to PCF coupling. However, for efficient coupling, the NA (~0.06 for large mode area PCFs) and spot sizes need to be matched to that of the SMF. Typical coupling efficiencies could be 40-50%.SMF splicing machines can also be adjusted to splice PCF fibers. Bennet et al [18], Xiao et al [19] and Chen et al [20] have described the process of achieving low loss splicing (0.05dB) to SMF fibers. The splicing process however will lead to microhole collapsing. Techniques for tapering large mode area PCFs without microhole collapse and for realizing selectively collapsed holes have also been reported in literature. [21, 22].

*Corresponding author: lathag@ssn.edu.in, pritanair@ssn.edu.in